Single Image Dehazing Using Bounded Channel Difference Prior

Xuan Zhao
Air-to-air Missile Research Institute
Luoyang, Henan, China
zxstud@163.com

Abstract

The single image dehazing task has made significant progress recently, aiming to recover the contrast and color of the scattered image. Many patch prior based dehazing methods have been explored, and this paper proposes another single image dehazing method by analyzing the prior information of local dehazed patches. With our observation, when the estimated transmission value varies from the ground-truth transmission value to 1, the output value of a metric function decrease correspondingly, which is defined based on the difference maps among three RGB channels of local dehazed patches normalized using global atmospheric light. Under additional bounding, the local transmission value can be estimated accurately. To reduce computation time, the whole image is divided into many small patches, and within each patch, we estimate a transmission value accurately. We further use weighted interpolation and guided filtering to refine the edges and details of the rough transmission map. Finally, we evaluate the proposed method using Fattal's synthetic haze images, SOTS dataset, and a wide variety of real-world haze images. Experiments show that our method outperforms other state-of-the-art dehazing algorithms by a large margin, especially on synthetic noisy haze images.

1. Introduction

1.1. Dehazing Task

Haze is a natural phenomenon caused by tiny particles in 3 the air, affecting the image's contrast and color greatly. The scattering level depends on the attenuation coefficient of the atmosphere and the distance between the camera and the object. Dehazing, aiming to recover the clean scene radiance, is an ill-posed problem due to the unknown transmission map and global atmospheric light. Early dehazing methods often need extra information, such as polarized filters and multiple images [22, 16], weather condition [15, 9], and depth information [14]. The applications of these methods are limited for requiring additional information. Recently, single image based dehazing methods have made significant progress, aiming to recover the clean image from the degraded input without additional information. Those methods can be roughly divided into two classes, respectively, prior based methods and data-driven methods.

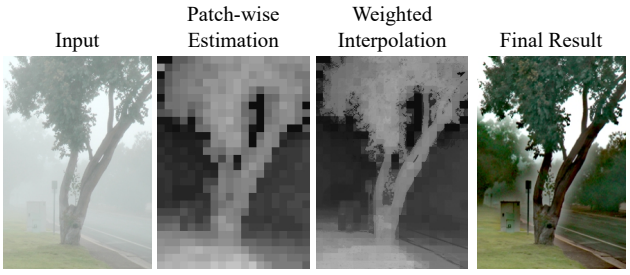

Figure 1. A dehazing example of the proposed local prior. We estimate the transmission map by dividing the input image into many small blocks (11×11). We use weighted interpolation and guided filtering to refine the structure of the rough transmission map. From the dehazing result, the proposed local prior yields excellent dehazing performance.

1.2. Prior Based Single Image Dehazing Methods

Many patch prior based dehazing methods have been explored. Fattal et al. [5] estimate transmission maps based on the assumption that transmission and surface shading are locally uncorrelated. He et al. [8] propose a classical dark channel prior (DCP) based on the observation of clean image that, as for most of natural clean image local patch, at least one color channel has very low intensity at some pixels. Some subsequent methods are proposed to solve the problems of DCP: Guided filtering [7] is proposed to replace time-consuming soft-matting [10];Meng et al. [13] employ boundary constraint and contextual regularization (BCCR) to refine the structure of rough transmission map; Chen et al [4] propose a robust dehazing method (GRM) which uses total generalized variation (TGV) to suppress artifacts. Besides, numerous dehazing methods based on the natural image prior have been proposed. Bayesian sta-

tistical method [17] model dehazing problem as a statistical model. Zhu et al. [18] find that in a hazy image, hazy degree of different image patch is relevant to color attenuation in a local patch, proposing color attenuation prior (CAP). Fattal et al. [6] propose a prior based dehazing method using color-lines (CL) and recover full transmission map by an augmented Markov Random Field model.

Different from patch based local prior, Berman et al. [2] find that local image patches with similar colors form a line from scene radiance to global atmospheric light and propose a non-local dehazing (NLD) method.

1.3. Data-Driven Single Image Dehazing Methods

Recently, data-driven methods have been explored in various image processing and computer vision tasks, including image dehazing. Tang et al. [24] model the dehazing into a learning framework to investigate haze-relevant features. Cai et al. [3] propose an end-to-end dehazing network (DehazeNet) using the synthetic hazy patches for transmission learning. Ren et al. [19, 21] propose a multi-scale CNN (MSCNN) that utilizes the image information of different spatial scales and coarse-to-fine scales. Li et al. [11] cast all dehazing processes into one network instead of estimating the transmission map (AOD-Net). Ren et al. [20] fuse three different pre-processing maps containing haze-relevant information with a progressive upsampling manner (GFN).

1.4. Motivations and Contributions

Similar to DCP, we assume that the local transmission values are constants. Given a hazy patch and the global atmospheric light, the ground-truth transmission value is between 0 and 1. When the estimated transmission value increases from the ground-truth value to 1, the color information of the dehazed patch degrades gradually. When the estimated transmission value decreases from the ground-truth value to 0, the pixel value range of the over-dehazed patch is out of the normal range. Using a proper bounding function, the local transmission value can be estimated accurately by analyzing the prior information of the difference maps among three RGB channels of dehazed patches normalized using global atmospheric light. To sum up, the main contributions of this paper are followings:

(1) We propose a novel local prior based single image dehazing method, which outperforms other state-of-the-art single image dehazing algorithms.

(2) We propose a fast implementation for the proposed method by dividing the whole image into many small patches.

(3) Experiments on Fattal's synthetic haze images show our method is robust to noise, different haze levels, and large objects.

2. Backgrounds

2.1. The Dehazing Task

The commonly used haze degradation model is described as [23]:

$$\mathbf{I}(x) = \mathbf{J}(x)\, t(x) + \mathbf{A}(1 - t(x)) \tag{1}$$

where $\mathbf{I}$ denotes input haze image, $\mathbf{J}$ denotes scene radiance, $\mathbf{A}$ represents global atmospheric light, x is the spatial image index, and t denotes transmission map related to the distance from the object to the camera. According to the Lambert Beer law when the atmosphere is homogeneous, the transmission map can be expressed as [23]:

$$t(x) = \exp(-\beta d(x)) \tag{2}$$

where β is the attenuation coefficient of the atmosphere, $d(x)$ represents the depth from object to camera, and x is the image index. By simply transforming the Eq. (1) , we can get:

$$\mathbf{J}(x) = \min\left\{\max\left\{\frac{\mathbf{I}(x) - \mathbf{A}}{t(x)} + \mathbf{A}, 0\right\}, 1\right\} \tag{3}$$

In order to get scene radiance, we should estimate t and $\mathbf{A}$ at first.

2.2. Dark Channel Prior

He et al. [8] propose a robust natural image prior based on the observation that as for clean natural images, the minimum of the local RGB patch is very close to zero:

$$\mathbf{J}^{dark}(x) = \min_{c\in\{r,g,b\}}\left(\min_{y\in\Omega(x)} J^c(y)\right) \approx 0 \tag{4}$$

where Ω denotes the local image patch, r, g, b is the RGB channel of the input image. Based on Eq. (4), the transmission map is estimated by applying dark channel operation on both sides of Eq. (1):

$$\tilde{t}(x) = 1 - \omega \min_{c\in\{r,g,b\}}\left(\min_{y\in\Omega(x)} \frac{I^c(y)}{A^c}\right) \tag{5}$$

where c is the color channel of RGB color space and ω is the parameter controlling the dehazing degree can be adjusted according to the haze level.

3. Proposed Method

3.1. The Observation

In the following parts, we assume that the global atmospheric light is known. Local prior based dehazing methods, such as DCP, usually establish the relations between the local transmission value and the local statics variables. We

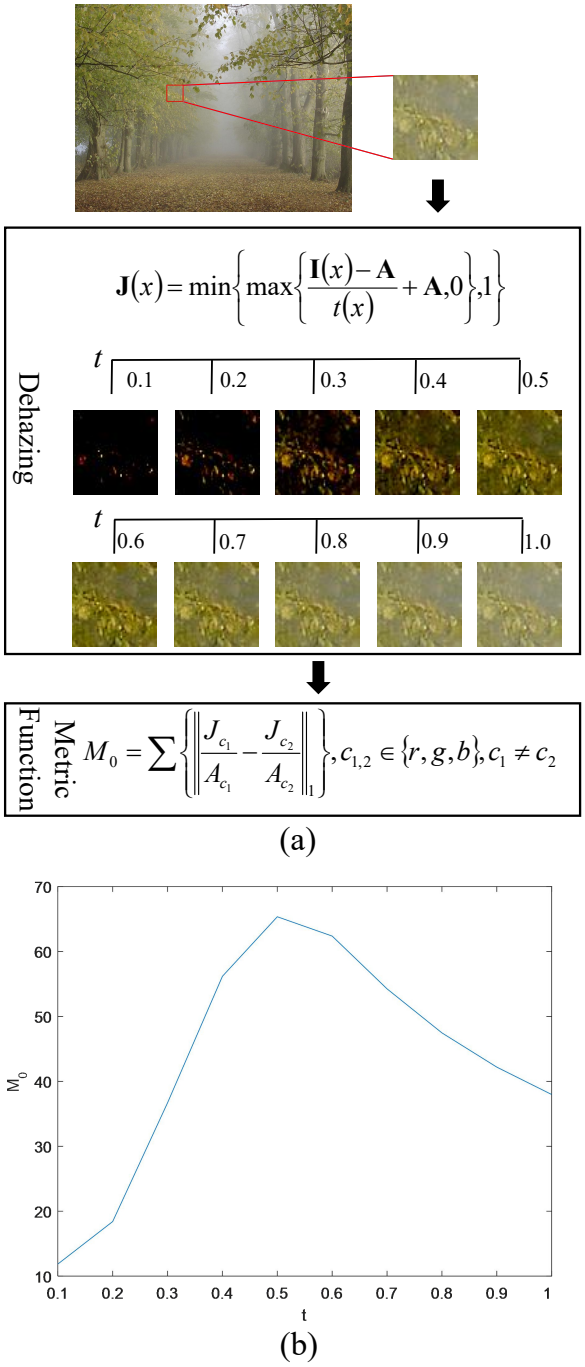

Figure 2. Illustration of the proposed local prior. (a) Dehazing examples of different transmission values of a randomly selected local haze patch (Eq. (3)). (b) The output values of the proposed metric function (Eq. (6)), taking the dehazed patches as the inputs. The proposed metric function is defined based on the channel difference maps among three normalized RGB channels of dehazed patches.

propose a novel local dehazing prior by analyzing the relation between the ground-truth transmission value and the dehazed patches under different transmission values. As shown in Fig. 2 (a), we show the dehazed patches of a randomly selected hazy patch. Furthermore, the dehazed patches are fed into the proposed metric function to compute the output values (M_0). From Fig. 2 (a), when t varies from 0.1 to 0.4, the dehazed patches are over-dehazed and many pixel values are close to 0; when t varies from 0.8 to 1.0, the dehazing performance is limited and the dehazed patches are still hazy. From Fig. 2 (b), the output value M_0 achieves the maximum when $t = 0.5$; from Fig. 2 (a), the dehazed patch also has good contrast and color when $t = 0.5$. To sum up, we aim to estimate the local transmission value using local prior information, which is formulated as a bounded metric function.

Given the global atmospheric light $A_c, c \in \{r, g, b\}$, the proposed metric function is defined as the sum of absolute values of difference maps among three normalized RGB channels of the dehazed patches:

$$M_0 = \left\|\frac{J_r}{A_r} - \frac{J_g}{A_g}\right\|_1 + \left\|\frac{J_r}{A_r} - \frac{J_b}{A_b}\right\|_1 + \left\|\frac{J_b}{A_b} - \frac{J_g}{A_g}\right\|_1 \quad (6)$$

where M_0 denotes the output value of metric function, $J_c, c \in \{r, g, b\}$ is the RGB channels of the dehazed patch. Combining Eq. (3) and Eq. (6), we will get the following formulation:

$$M_0 = \left\|\left(\frac{I_r}{A_r} - \frac{I_g}{A_g}\right)\frac{1}{t}\right\|_1 + \left\|\left(\frac{I_r}{A_r} - \frac{I_b}{A_b}\right)\frac{1}{t}\right\|_1 + \left\|\left(\frac{I_b}{A_b} - \frac{I_g}{A_g}\right)\frac{1}{t}\right\|_1 \quad (7)$$

From Eq. (7), the value of M_0 increases when t decreases. However, from Fig. 2 (a), the over-dehazed patches are close to zero, leading to low M_0. Therefore, taking the dehazed patches as the input data, the maximum of output values of Eq. (6) is correlated with the best transmission value. To demonstrate the analysis of Eq. (7), we test the values of M_0 using synthetic haze patches with different global atmospheric light and transmission values, as shown in Fig. 3. From Fig. 3 (c), the output value of Eq. (7) decreases when the transmission value decreases, proving the analysis of color information when t varies from the ground-truth value to 1 (taking I as the input data).

3.2. Dehazing Using Additional Bounding

Based on Eq. (3), when t is close to 0, the values of dehazed patch J are close to 0 or 1. Therefore, the Eq. (6) is not robust for extreme colorful cases, such as $J_r(x) = 1, J_g(x) = 1, J_b(x) = 0$. In such cases, the hazy patches are usually over-dehazed. To solve the problem of extreme colorful cases, additional bounding is needed, which can be regarded as a regularization term:

$$M = M_0 + R(J) \quad (8)$$

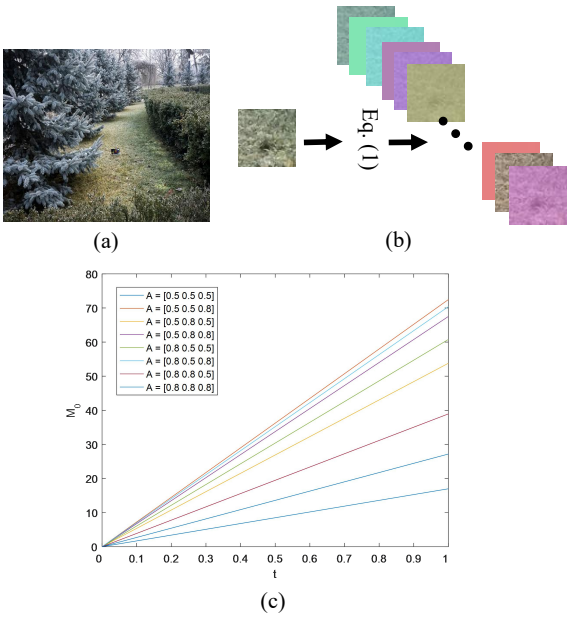

Figure 3. (a) A haze-free image from NH-HAZE dataset [1]. (b) Synthetic hazy patches with random global atmospheric light and transmission values based-on the Eq. (1). (c) The output values of Eq.(7). Compared with hazy patches ($t < 1$), the haze-free patch has higher M_0, meaning more color information.

As for the dehazed patches, we reject the existence of the value 0:

$$R(J) = \mathbf{F}\left(\frac{J_{c_1}}{J_{c_2}}\right), c_{1,2} \in \{r, g, b\}, c_1 \neq c_2 \qquad (9)$$

where $\mathbf{F}$ denotes the checking function: if there exists 0 in the dehazed patches, the output value of Eq. (8) will become to $\pm\infty$, which is not included for the estimation of the transmission value. It is also easy to avoid interfere from the input haze image:

$$\hat{I} = \max(I, \epsilon) \qquad (10)$$

where ϵ denotes a small positive threshold. With equation (**??**), the local transmission value can be estimated by maximizing the bounded metric function:

$$\tilde{t} = \max_t M_0 + R(J), t \in (\epsilon, 1) \qquad (11)$$

where $\tilde{t}$ denotes the estimated transmission value.

A dehazing example of several synthetic haze patches is shown in Fig. 4. Four haze-free patches are selected from the clean image shown in Fig. 3 (a). To test the dehazing performance of the proposed method, we choose two different haze levels (dense haze:$t = 0.3$, light haze:$t = 0.8$). We use the grid search method to solve the problem (11). When t is set as 0.3, the estimated transmission values of four hazy patches are all very close to the 0.3; When t is set as 0.8,

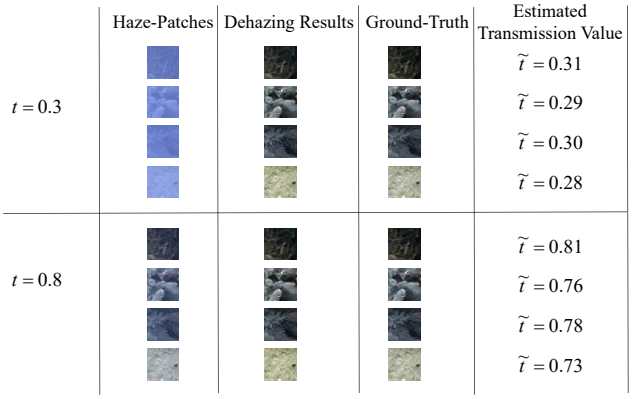

Figure 4. Dehazing examples of several synthetic patches (40×40). The ground-truth patches are randomly selected from Fig. 3 (a). From the fifth column, the transmission values are estimated using Eq. (11). The global atmospheric light for three RGB channels is set as $\{0.5, 0.6, 1.0\}$.

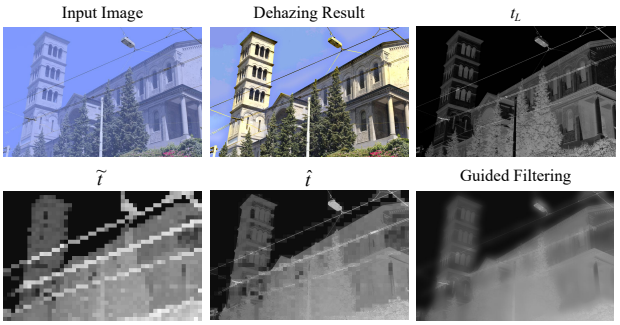

Figure 5. Rough transmission map refinement. From the second row, the edge of $\hat{t}$ is much better than $\tilde{t}$ after weighted interpolation using Eq. (14).

the dehazed patches are also very close to the ground-truth patches. Generally, the proposed dehazing prior is robust to different haze levels.

A haze image may contain haze-free regions. Taking the clean patches as the inputs, the mean output value of Eq. (8) will be a small positive value. In this condition, the estimated local transmission is unstable. Therefore, the transmission value is set as 1 if the mean output value of Eq. (8) is smaller than a low threshold (0.1).

3.3. Fast Implementation

Given a high-resolution haze image, it is time-consuming to estimate the transmission value pixel-by-pixel. To save running time, we design a block-wise method for fast transmission map estimation. The whole image is divided into small blocks with fixed size (such as 21×21), and each block is used to estimate a local transmission value. As shown in Fig. 1, within each block the transmission is regarded as a constant. Then, the rough transmission map can be refined using the guided filtering process the

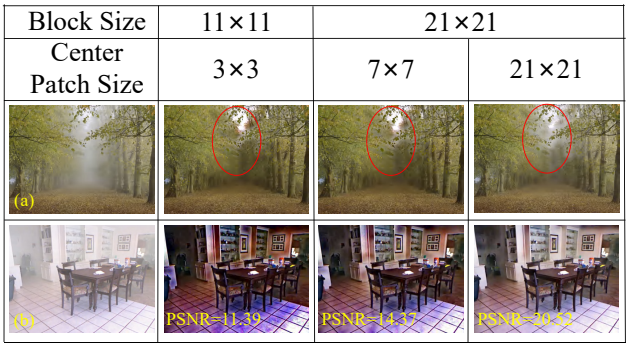

Figure 6. Block/center-patch size selection examples. For natural haze image (a), the local transmission value can be estimated well with small a center patch size. However, for challenging synthetic haze image (b) from SOTS [12], we use the whole block to estimate the local transmission value.

Table 1. Running time table of different block (B_i) sizes, center patch (P_i) sizes, and resolutions.

Resolution	B_i:21 × 21		Pixel-Wise
	P_i:7 × 7	P_i:21 × 21	P_i:7 × 7
300 × 300	2.82	3.61	112.35
500 × 500	7.18	8.94	324.20
700 × 700	15.92	19.74	595.14
900 × 900	26.24	31.07	969.08

same as DCP does. However, to reduce the artifacts caused by block-wise division, we design a weighted interpolation method to refine the rough transmission map at first.

At first, given the global atmospheric light, we calculate the low boundary value of the transmission map. The scene radiance should be larger than 0:

$$\mathbf{J}(x) = \frac{\mathbf{I}(x) - \mathbf{A}}{t(x)} + \mathbf{A} \geq 0 \tag{12}$$

From Eq. (12), we can get the following formulation:

$$t(x) \geq 1 - \min_{c \in \{r,g,b\}} \frac{I_c(x)}{A_c} = t_L \tag{13}$$

For each pixel of the rough transmission map, we search the N closest blocks B_i ($i \in \{1, ..., N\}$, N denotes the number of the blocks). Then, the final transmission map is computed using the weighted average value:

$$\hat{t}(x_0) = \frac{\sum_{i=1}^{N} \mathbf{exp}\{\frac{\|t_L(x_0) - t_L(x_i)\|_1}{\sigma_I}\} \min\{\tilde{t}(x_i), \tilde{t}(x_0)\}}{\sum_{i=1}^{N} \mathbf{exp}\{\frac{\|t_L(x_0) - t_L(x_i)\|_1}{\sigma_I}\}} \tag{14}$$

where x_0 denotes the current pixel location, x_i denotes the spatial pixel location of the block center, σ_I is set as constant. With Eq. (14), the boundary of the estimated rough transmission map is refined using t_L. Then, the refined transmission map is fed into the guided filtering process for further refinement. An example of Eq. (14) is shown in Fig. 5. From Fig. 5, rough transmission map $\tilde{t}$ may cause block artifacts close to the edge. Compared with $\tilde{t}$, $\hat{t}$ has better edge information.

Table 2. Block/Patch Size Selection

Dataset	Block Size	Center Patch Size
Fattal	21	7
SOTS	21	21
Real-Images	11	3

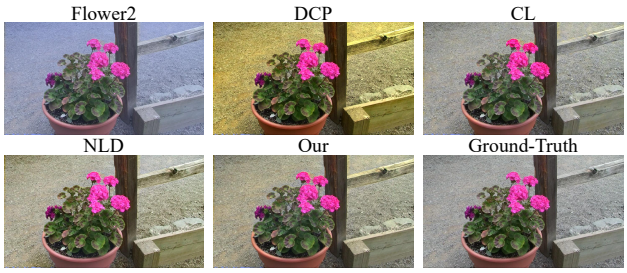

Figure 7. Dehazing results of the haze image Flower2.

3.4. Block/Center-Patch Size Selection

To save computation time, the whole image is divided into many small blocks. With our observation, however, in some conditions, the transmission value can also be estimated well when we use 7×7 center patch P_i of 21×21 block B_i. For natural haze images, the small center patch can be used to further decrease running time and reduce artifacts close to the edges; for images containing sky region, white objects, or large homogeneous regions, it is suggested that the whole block B_i should be used.

Fig. 6 shows two examples of block/center-patch size selection. For haze image (a) in Fig. 6, the dehazing result has the best dehazing performance when block size and center patch size is set as 11×11 and 3×3 respectively. For haze image (b) in Fig. 6, the dehazing result has the highest PSNR when the whole block is used for the estimation of the local transmission value.

Running times of different blocks and center patch sizes are shown in table 1. For high resolution 900×900 haze image, our implementation achieves $30\times$ speeding up.

4. Experiments

To prove the performance, we evaluate the proposed dehazing method using Fattal's synthetic dataset [6] and 500 SOTS [12] haze images. We also show qualitative results of a wide variety of real-world haze images. Similar to section 3.1, we assume that global atmospheric light is known. σ_I in Eq. (14) is set as -100. The patch size setting for transmission map estimation can be found in table 2. Three state-of-the-art prior based dehazing methods are selected for quantitative and qualitative comparison, including DCP(dark channel prior) [8], NLD(non-local de-

Table 3. L_1 error table of synthetic haze images with different scenarios. The pixel value is normalized into $[0, 1]$.

Image	DCP	CL	NLD	Our
Road1	0.0432	**0.0278**	0.0325	0.0339
Road2	0.0469	**0.0313**	0.0459	0.0330
Flower1	0.0981	**0.0187**	0.0437	0.0354
Flower2	0.0945	**0.0151**	0.0387	0.0309
Lawn1	0.0506	0.0306	0.0444	**0.0298**
Lawn2	0.0560	**0.0280**	0.0417	0.0290
Mansion	0.0416	**0.0218**	0.0400	0.0296
Couch	0.0410	0.0533	0.0507	**0.0308**
Moebius	0.1465	0.0757	0.0669	**0.0580**
Reindeer	0.0682	0.0336	0.0589	**0.0244**
Average	0.0687	**0.0336**	0.0463	**0.0335**

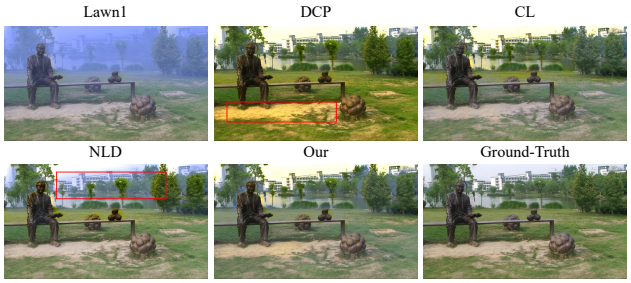

Figure 8. Dehazing results of the haze image Lawn1.

hazing) [2], and CL(color lines) [6]. Three state-of-the-art learning-based methods are used for quantitative comparison on SOTS dataset, including MSCNN [19], AOD-Net [11], and GFN [20]. To keep fair, for synthetic haze images, we do not include gamma correction and pixel value clipping for the dehazing results of NLD and our method. The parameters of NLD and our method are set as constants for quantitative comparison. For qualitative comparison, the global atmospheric light and gamma correction parameters are the same for all methods (for haze image Train, we adjust the global atmospheric light slightly). The dehazing results of DCP and CL can be obtained on Fattal's online project webpage.

4.1. Quantitative Results

4.1.1 Different Scenarios

Firstly, we evaluate the proposed dehazing method using ten synthetic haze images with different scenarios. Because the proposed dehazing prior is a local patch based prior, dehazing performance on large objects is meaningful.

Quantitative Results of ten synthetic haze images are shown in Table. 4, and we compute the L_1 errors on non-sky pixels of dehazed images. Obviously, our dehazing method is robust for a wide variety of scenarios and outperforms DCP and NLD on most haze images by a large margin. Moreover, our method achieves the lowest average L_1 error,

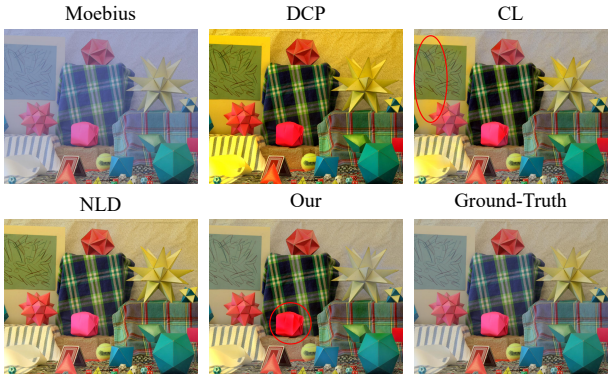

Figure 9. Dehazing results of the haze image Moebius.

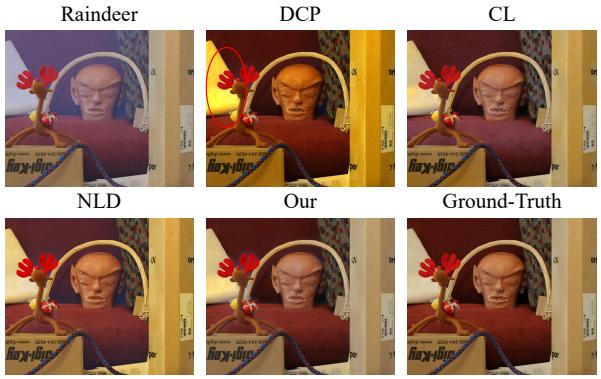

Figure 10. Dehazing results of the haze image Raindeer.

which is competitive to the state-of-the-art dehazing method based on color lines (CL[6]).

Dehazing results of the haze image Flower2 is shown in Fig. 7. Due to inaccurate low values of the estimated transmission map, the dehazing result of DCP has a yellow hue. Compared with NLD, our local prior based method achieves higher performance. The ground in haze image Flower2 can be regarded as a large object, demonstrating the performance of the proposed local prior for large objects. The gamma correction based method [6] can be used to remedy inaccurate low values of the estimated transmission map.

Dehazing results of the haze image Lawn1 are shown in Fig. 8. As for the dehazing results of DCP and NLD, the region in the red box is over-dehazed and hazy respectively. Due to similar colors, the clustering results are not reliable, causing poor dehazing performance.

From Fig. 9, the dehazing result of DCP is over-saturated seriously. The region in the red ellipse of the dehazing result of CL is also over-saturated. Compared with NLD, our result achieves better performance, despite the over-dehazed region in the red circle.

Dehazing results of the haze image Raindeer are shown in Fig. 10. The region in the red circle of the dehazing result of DCP is over-saturated. Compared with CL and NLD, our result is more close to the ground-truth.

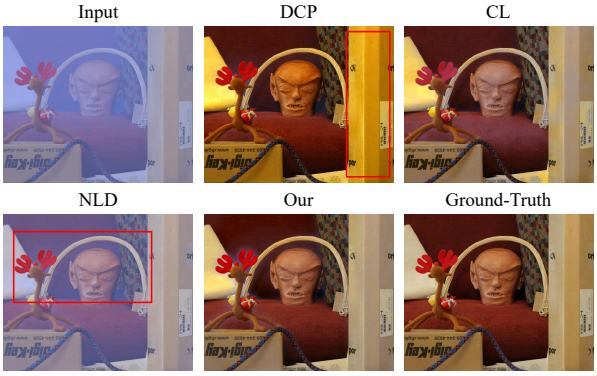

Figure 11. Dehazing results of the heavy haze image Raindeer. Compared with other methods, our result is more close to the ground-truth.

Table 4. L_1 error of synthetic images under different scattering levels. The pixel value is normalized into $[0, 1]$. Low: low scattering level; Middle: Middle scattering level; High: high scattering level. The error is computed between dehazed images and clean ground-truth images.

Image	Level	DCP	CL	NLD	Our
Road1	low	0.0386	0.0218	0.0506	**0.0218**
	middle	0.0432	**0.0283**	0.0313	0.0350
	high	0.0539	**0.0338**	0.1551	0.0428
Lawn1	low	0.0581	**0.0151**	0.0315	0.0160
	middle	0.0560	0.0301	0.0444	**0.0298**
	high	0.0620	0.0354	0.1529	**0.0311**
Mansion	low	0.0429	**0.0152**	0.0750	0.0212
	middle	0.0416	**0.0221**	0.0400	0.0296
	high	0.0453	**0.0310**	0.1666	0.0401
Church	low	0.0398	**0.0125**	0.0441	0.0255
	middle	0.0315	**0.0160**	0.0369	0.0286
	high	0.0304	**0.0256**	0.1320	0.0321
Raindeer	low	0.0674	0.0237	0.0622	**0.0101**
	middle	0.0682	0.0350	0.0589	**0.0244**
	high	0.0701	0.0434	0.1890	**0.0342**
Average	-	0.0499	**0.0259**	0.0847	0.0282

4.1.2 Varying Scattering/Noise Levels

Following the online experiment results [6], we evaluate the proposed dehazing method using haze images with varying scattering/noise levels. From Table. 4, our dehazing method outperforms DCP and NLD and is competitive to CL. Dehazing results of the heavy haze image Raindeer are shown in Fig. 11. From the first row of Fig. 11, the dehazing result of DCP is oversaturated and the image region in the red box has the yellow hue. From the second row, the rehazing result of NLD is still hazy due to degraded color information. The whole color information of the input heavy haze image is limited and clustering results of NLD are unreliable.

Table 5 shows L_1 errors of DCP, NLD, CL, and our methods under three different noise levels. It is obvious that our dehazing results outperform other methods by a large margin, demonstrating the performance of the proposed local prior to noisy haze images. Dehazing results of the haze image Mansion ($\sigma = 0.05$) are shown in Fig. 13.

Table 5. L_1 error of dehazed images under different noise levels. The pixel value is normalized into $[0, 1]$. The error is computed between dehazed images and clean ground-truth images.

Image	σ	DCP	CL	NLD	Our
Road1	0.01	0.0489	**0.0319**	0.0344	**0.0360**
	0.025	0.0621	0.0542	0.0483	**0.0452**
	0.05	0.0900	0.0960	0.0795	**0.0738**
Lawn1	0.01	0.0589	0.0332	0.0430	**0.0320**
	0.025	0.0681	0.0575	0.0506	**0.0427**
	0.05	0.0897	0.1064	0.0895	**0.0687**
Mansion	0.01	0.0389	**0.0290**	0.0434	0.0310
	0.025	0.0433	0.0493	0.0575	**0.0385**
	0.05	0.0729	0.0777	0.0833	**0.0621**
Church	0.01	0.0324	**0.0284**	0.0378	0.0299
	0.025	0.0384	0.0530	0.0444	**0.0334**
	0.05	0.0640	0.0891	0.0628	**0.0530**
Raindeer	0.01	0.0656	0.0419	0.0589	**0.0264**
	0.025	0.0671	0.0536	0.0638	**0.0375**
	0.05	0.0853	0.0834	0.0879	**0.0671**
Average	-	0.0617	0.0590	0.0590	**0.0452**

Table 6. PSNR/SSIM table of different dehazing methods on SOTS Dataset.

Model	Method	SOTS	
		PSNR	SSIM
Prior-based	DCP	16.62	0.818
	BCCR	16.88	0.791
	NLD	17.29	0.749
	Our	20.83	**0.883**
Learning-based	MSCNN	17.57	0.810
	AOD-Net	19.06	0.850
	GFN	**22.30**	0.880

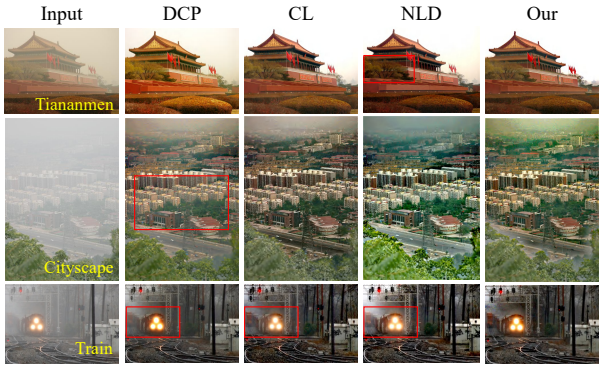

Figure 12. Dehazing results of real-world haze images Train, Cityscape, and Tiananmen.

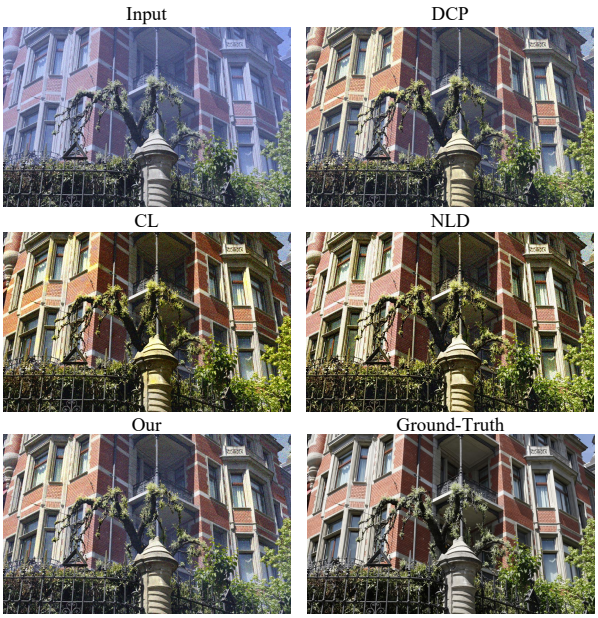

Figure 13. Dehazing results of the haze image Mansion with high noise level ($\sigma = 0.05$).

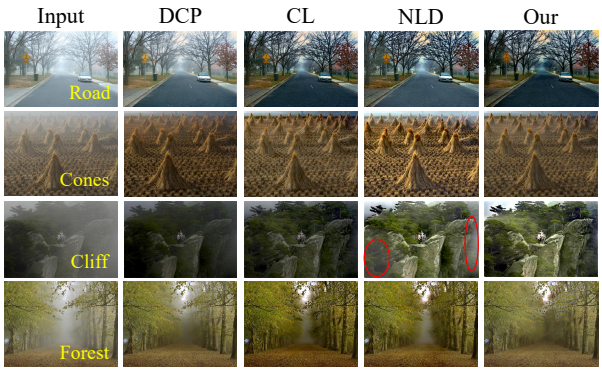

Figure 14. Dehazing results of real-world haze images Road, Flags, Cones, and Cliff. For dehazing result of the haze image Cliff, we clip the 0.5% of the pixel values both in the shadows and in the highlights.

Figure 15. Dehazing results of high-resolution real-world haze image Herzelya.

4.1.3 Results On SOTS Dataset

SOTS Dataset is used for further comparison with other state-of-the-art dehazing methods. From table 6, our method achieves the highest average SSIM value and the second-highest average PSNR value on SOTS dataset, which outperforms DCP, BCCR, and NLD by a large margin.

For SOTS datasets, our prior based dehazing method is not as well as GFN, which is well designed and trained using many synthetic haze images. Despite the weaker performance, our methods can generate reasonable haze-free clean images on a wide variety of real-world haze images. The dehazing performance of deep learning based dehazing methods is limited to unseen scenes.

4.2. Qualitative Results

Visual quality and dehazing performance of dehazed results on real-world haze images are important for evaluating dehazing methods. In this part, we show the dehazing results of many real-world haze images.

Dehazing results of haze image Train, Tiananmen, and Cityscape are shown in Fig. 12. From the left column to the right column are input haze image, dehazing results of DCP, CL, NLD, and our method. The dehazing results of DCP still seem to be dim, such as the image regions in the red boxes of Train and Cityscape. For the dehazing result of NLD on haze image Tiananmen, the tree in red box region looks dark and has poor contrast. From the third row, the image regions in red boxes of dehazing results of DCP, CL, and NLD are not as clear as our result, demonstrating the dehazing performance of the propsoed method.

Fig. 14 shows dehazing results of haze image Road, Cones, Cliff, and Forest. Compared with DCP, CL, NLD, our dehazing results of haze image Cones and Forest are more clear, especially on regions with farther depth information. From the third row of Fig. 14, the proposed local prior yields excellent dehazing performance on haze image Cliff. The image areas in the red ellipses of dehazing result of NLD on the haze image Cliff are still hazy. Additionally, we show a high-resolution dehazing case in Fig. 15, and the proposed local dehazing prior recovering the color and details of objects well.

5. Conclusion

In this paper, we propose a novel local prior for the single image dehazing task. We find that the haze level of the local haze patch can be evaluated using a carefully designed metric function, called channel difference prior. Besides, additional bounding is used to avoid over-dehazing. To save computation time, we design a fast block based algorithm for transmission map estimation. Experiments on synthetic and real-world haze images demonstrate the state-of-the-art performance of the proposed dehazing method.

References

[1] Codruta O. Ancuti, Cosmin Ancuti, and Radu Timofte. NH-HAZE: an image dehazing benchmark with non-homogeneous hazy and haze-free images. In *Proceedings of the IEEE Conference on Computer Vision and Pattern Recognition Workshops*, IEEE CVPR 2020, 2020. 4

[2] Dana Berman, Tali Treibitz, and Shai Avidan. Non-local image dehazing. In *Proc. IEEE Conf. Comput. Vis. Pattern Recognit. (CVPR)*, pages 1674–1682, 2016. 2, 6

[3] B. Cai, X. Xu, K. Jia, C. Qing, and D. Tao. Dehazenet: An end-to-end system for single image haze removal. *IEEE Trans. Image Process.*, 25(11):5187–5198, Aug. 2016. 2

[4] Chen Chen, Minh N. Do, and Jue Wang. Robust image and video dehazing with visual artifact suppression via gradient residual minimization. In *Proc. Eur. Conf. Comput. Vision*, pages 576–591, 2016. 1

[5] Raanan Fattal. Single image dehazing. *ACM Trans. Graph.*, 27(3):1–9, 2008. 1

[6] Raanan Fattal. Dehazing using color-lines. *ACM Trans. Graph.*, 34(1), 2014. 2, 5, 6, 7

[7] Kaiming He, Jian Sun, and Xiaoou Tang. Guided image filtering. *IEEE Trans. Pattern Anal. Mach. Intell.*, 35(6):1397–1409, Oct. 2013. 1

[8] K. He, J. Sun, and X. Tang. Single image haze removal using dark channel prior. *IEEE Trans. Pattern Anal. Mach. Intell.*, 33(12):2341–2353, Sep. 2011. 1, 2, 5

[9] Johannes Kopf, Boris Neubert, Billy Chen, Michael Cohen, Daniel Cohen-Or, Oliver Deussen, Matt Uyttendaele, and Dani Lischinski. Deep photo: Model-based photograph enhancement and viewing. *ACM Trans. Graph.*, 27(5):73–82, 2008. 1

[10] A. Levin. A closed form solution to natural image matting. In *Proc. IEEE Conf. Comput. Vis. Pattern Recognit. (CVPR)*, volume 1, pages 61–68, 2006. 1

[11] Boyi Li, Xiulian Peng, Zhangyang Wang, Jizheng Xu, and Feng Dan. Aod-net: All-in-one dehazing network. In *Proc. IEEE Int. Conf. Comput. Vis.*, pages 4780–4788, 2017. 2, 6

[12] B. Li, W. Ren, D. Fu, D. Tao, D. Feng, W. Zeng, and Z. Wang. Benchmarking single-image dehazing and beyond. *IEEE Transactions on Image Processing*, 28(1):492–505, 2019. 5

[13] Gaofeng Meng, Ying Wang, Jiangyong Duan, Shiming Xiang, and Chunhong Pan. Efficient image dehazing with boundary constraint and contextual regularization. In *Proc. IEEE Conf. Comput. Vis. Pattern Recognit. (CVPR)*, pages 617–624, 2014. 1

[14] Srinivasa Narasimhan and Shree Nayar. Interactive (de)weathering of an image using physical models. *Proc. IEEE Workshop Color Photometric Methods Comput. Vis.*, 10, 12 2015. 1

[15] Srinivasa G. Narasimhan and Shree K. Nayar. Chromatic framework for vision in bad weather. In *Proc. IEEE Conf. Comput. Vis. Pattern Recognit. (CVPR)*, volume 1, pages 598–605, 2000. 1

[16] S. G. Narasimhan and S. K. Nayar. Contrast restoration of weather degraded images. *IEEE Trans. Pattern Anal. Mach. Intell.*, 25(6):713–724, June 2003. 1

[17] Ko Nishino, Louis Kratz, and Stephen Lombardi. Bayesian defogging. *Int. J. Comput. Vis.*, 98(3):263–278, Jul. 2012. 2

[18] Qingsong, Zhu, Jiaming, Mai, Ling, and Shao. A fast single image haze removal algorithm using color attenuation prior. *IEEE Trans. Image Process.*, 24(11):3522–3533, Nov. 2015. 2

[19] Wenqi Ren, Si Liu, Hua Zhang, Jinshan Pan, Xiaochun Cao, and Ming-Hsuan Yang. Single image dehazing via multi-scale convolutional neural networks. In *Proc. Eur. Conf. Comput. Vis.*, pages 154–169, 2016. 2, 6

[20] W. Ren, L. Ma, J. Zhang, J. Pan, X. Cao, W. Liu, and M. Yang. Gated fusion network for single image dehazing. In *Proc. IEEE Conf. Comput. Vis. Pattern Recognit. (CVPR)*, pages 3253–3261, 2018. 2, 6

[21] Wenqi Ren, Jinshan Pan, Hua Zhang, Xiaochun Cao, and Ming-Hsuan Yang. Single image dehazing via multi-scale convolutional neural networks with holistic edges. *International Journal of Computer Vision*, 128, Jan. 2020. 2

[22] Y. Y. Schechner, S. G. Narasimhan, and S. K. Nayar. Instant dehazing of images using polarization. In *Proc. IEEE Conf. Comput. Vis. Pattern Recognit. (CVPR)*, volume 1, page 325, 2001. 1

[23] Robby T. Tan. Visibility in bad weather from a single image. In *Proc. IEEE Conf. Comput. Vis. Pattern Recognit. (CVPR)*, volume 1, page 1–8, June 2008. 2

[24] Ketan Tang, Jianchao Yang, and Jue Wang. Investigating haze-relevant features in a learning framework for image dehazing. In *Proc. IEEE Conf. Comput. Vis. Pattern Recognit. (CVPR)*, pages 2995–3002, 2014. 2